JES Focus Issue on Mathematical Modeling of Electrochemical Systems at Multiple Scales in Honor of John Newman

# Reducing Inhomogeneous Current Density Distribution in Graphite Electrodes by Design Variation

**Frank M. Kindermann,[a,*,z] Patrick J. Osswald,[a] Günter Ehlert,[a] Jörg Schuster,[b,*] Alexander Rheinfeld,[a,*] and Andreas Jossen[a]**

[a]*Technical University of Munich (TUM), Institute for Electrical Energy Storage Technology, Munich, Germany*
[b]*Technical University of Munich (TUM), Chair of Technical Electrochemistry, Garching, Germany*

Inhomogeneous utilization of electrodes and consequent limitations in the operating conditions are a severe problem, reducing lifetime and safety. By using a previously developed laboratory cell setup, we are able to show an inhomogeneous retrieval of lithium-ions from a graphite electrode throughout the layer with spatial resolution for two different graphites. After provoking inhomogeneities via constant current operations, equilibration processes are recorded and are assigned to two different effects. One effect is an equilibration inside the particles (intra-particle) from surface to bulk whereas the second effect is an equalization between the particles (inter-particle) to reach a homogeneous degree of lithiation in each particle throughout the electrode layer. With the recorded data, we implemented a P2D model with multiple particle sizes and considered the electrode thickness in several separate domains. Using the relaxation data of intra- and inter-particle relaxation for parametrizing the model, we investigated the influence of different solid and liquid phase parameters. As the liquid phase parameters scaled via porosity and tortuosity showed the biggest impact, we performed a design variation study to achieve a more homogeneous utilization of the electrode. Structuring the electrode to lower tortuosity is identified as the most promising design variation for homogeneous utilization.


Manuscript submitted February 20, 2017; revised manuscript received April 18, 2017. Published April 28, 2017. *This paper is part of the JES Focus Issue on Mathematical Modeling of Electrochemical Systems at Multiple Scales in Honor of John Newman.*

Lithium-ion cells are the electrochemical power source of choice, not only for portable electronic devices but also for plug-in hybrid electric vehicles (PHEVs) and electric vehicles (EVs). Despite significant improvements regarding energy density and cycle stability, drawbacks remain, preventing the acceptance of EVs as a coequal alternative to internal combustion engine vehicles.

Resulting from advancements in the quality of manufacturing processes, the ratio between active and inactive components could be improved by realizing thicker electrode coatings and thinner current collector foils.[1] This increase in the energy density of the cells, however, comes with longer charging times due to a reduced rate capability. While concepts such as intelligent charging strategies require a comprehensive framework to be implemented,[2] the most obvious approach is to increase the charging power. As presented by Tesla's Supercharger concept, the battery is charged up to 80% state of charge (SOC) within 40 min using a charging power of up to 120 kW.[3] The high charging power requires high charging currents due to current limitations for 400 V high voltage on-board power systems.

Various publications address the variations in current density distribution and the resulting SOC inhomogeneities. The impact of the cell design and the resulting equalization processes along the electrodes are presented using experimental cells[4–11] or by a modeling approach.[12,13] The resulting inhomogeneous utilization of the active material leads to undesired side reactions and accelerated degradation, especially lithium plating[14,15] and an uneven mechanical expansion of the anode.[16] This is further provoked by the increasing thickness of the cell's electrodes. In contrast to the equalizing process along the electrode, only limited knowledge regarding the process throughout the electrode thickness are available.

Consequently, a fundamental understanding of the lithium-ion transport mechanisms is a crucial requirement to enable intelligent fast charging strategies. In our previous work,[17] a hypothesis was presented, discussing possible lithium-ion relaxation processes inside a lithium-ion cell. The first effect is an equilibration inside the particles, where the concentration gradient between the bulk and the surface of graphite particles leads to an intra-particle equalization process. The second effect addresses the equalization between different particles (inter-particle), where the equalization of the lithium-ion concentration gradient occurs through the electrolyte. This equalization was successfully observed using an experimental test cell, where the anode consisted of three separated graphite layers[18] based on the works of La Mantia et al.,[19] Ng et al.[20] and Klink et al.[21,22] During normal operation, the layers were connected and performed as a single electrode. After full lithiation, a charge step was performed and the layers, based on the geometric proximity to the counter electrode, provided an unequal amount of the required charge. After switching off the current, the potential of all three layers was observed individually and the equalization currents between the single layers were measured.

In this paper we show measurements of inhomogeneous extraction of lithium-ions and following equalization processes for two different types of graphite. With these data we implement a P2D model with three separated electrodes to study the influence of several solid and liquid phase parameters on the observed current density distribution. According to the investigated parameters, we perform a design variation study to achieve a more homogeneous utilization.

## Experimental and Measurements

The measurement data were gathered with a previously presented laboratory cell design called multi-layer cell (MLC).[21] These data was then used to parametrize our model for a consecutive design variation study.

***Experiment.—***In addition to our previous work that was carried out on a graphite with a D50 value of 19 µm (referred to as large particle graphite – LG), we repeated the same equilibration measurements after an inhomogeneous utilization of the electrodes for a smaller particle graphite with a D50 value of 2.3 µm (small particle graphite – SG) according to the manufacturer. The experimental setup can be seen in Figure 1 and is described in more detail in Reference 18.

Both graphites were processed in a similar fashion. The graphite containing slurry and PVdF binder (polyvinylidene fluoride; Sigma-Aldrich) were mixed in a 95:5 wt ratio in NMP (N-methylpyrrolidone;

*Electrochemical Society Student Member.
[z]E-mail: f.kindermann@tum.de

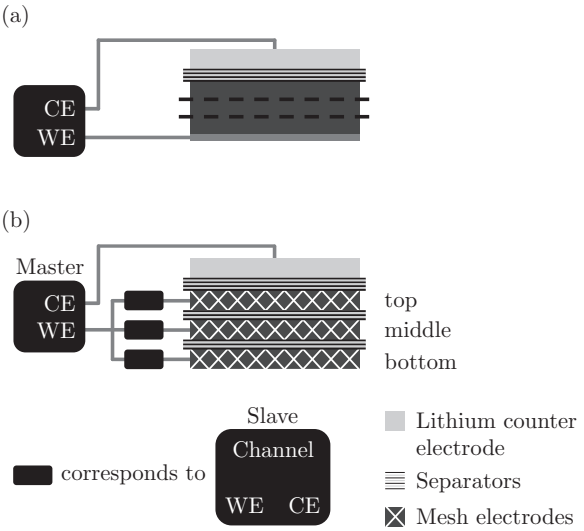


**Figure 1.** Scheme of cell setup showing (a) the cross section of a typical half-cell measurement versus a lithium-metal counter electrode (CE). The dashed lines represent the exemplary sectioning of this electrode which is implemented in (b) with each layer being connected to a single potentiostat – called slave channels. A separate master channel is used for applying the "cell current" between the lithium counter electrode and the three working electrodes (WE).[18,21]

Sigma-Aldrich) solvent. The slurry was coated by an automatic coater (RK Print) on a Microgrid Cu25 copper mesh (provided by Dexmet Corporation) in the case of LG and on a MC33 copper mesh (Precision Eforming Ltd.) in the case of SG. The coating speed for both coatings was 1.5 m min$^{-1}$. The LG electrodes were compressed for 2 min with 2.5 t, whereas the SG electrodes were not treated due to mechanical instabilities arising during the pressing process. Porosities for both kinds of electrodes were calculated and respective tortuosities were measured as suggested by Landesfeind et al.[23] All properties comparing both electrode disks that were punched out with 15 mm in diameter are listed in Table I.

**Table I. Properties of electrode disks from SG and LG. All values are measured or consequently calculated.**

| | SG | LG |
|---|---|---|
| **Material properties** | | |
| D10 value | 0.9 µm | 7 µm |
| D50 value | 2.3 µm | 19 µm |
| D90 value | 5.7 µm | 47 µm |
| Mesh thickness | 9 µm (MC33) | 24 µm (Microgrid Cu25) |
| **Electrode properties** | | |
| Coating thickness | 70 µm | 60 µm |
| Resulting thickness | 42.5 ± 1 µm | 44 ± 1 µm |
| Porosity | 79 ± 2 % | 32 ± 2 % |
| Tortuosity | 3.7 ± 0.5 | 4.9 ± 0.5 |
| Graphite loading | 1.82 mg cm$^{-2}$ | 4.13 mg cm$^{-2}$ |
| Capacity per disk | 1.20 mA h | 2.48 mA h |

***Measurement comparison.***—By using the setup shown in Figure 1 with three electrode disks separated by a Celgard 2325 separator, we are able to measure the capacity going in or out of each layer

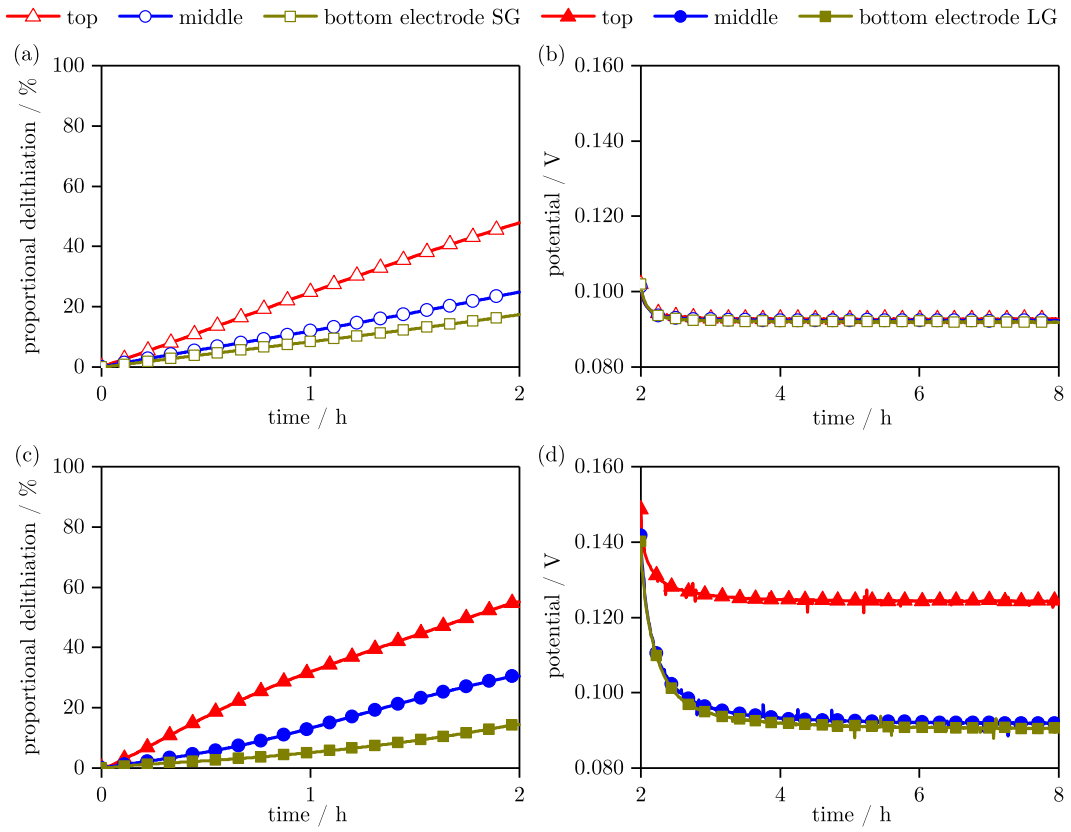


**Figure 2.** Comparison of SG (upper array) and LG (lower array) with respect to input capacity to each layer during 2 h delithiation process with C/10 current shown as percentage of overall capacity ((a) and (c)) and following intra-particle potential relaxation where no charge is exchanged between the layers ((b) and (d)). As can be seen, the disks were not delithiated equally by 33.3% but quite inhomogeneously. The most obvious effect can be seen in (d) as the top electrode of the LG was discharged that much more than the lower two electrodes that it relaxes to a stage-2 potential whereas the lower two electrodes stay in stage-1.

during a half-cell measurement mode and can additionally measure the potential of each disk versus $Li/Li^+$.

When comparing both graphites incorporated in a MLC setup during delithiation with a C/10 current for 2 h from a fully lithiated state, we can see that the SG electrodes show a more homogeneous utilization (Figure 2a and 2c) and a faster intra-particle relaxation (Figure 2b and 2d). The more homogeneous utilization with all particles still in the same lithiation stage (Figure 2b) is probably due to lower gradients in the electrolyte potential that come with the higher porosity and, therefore, lower tortuosity. The faster intra-particle equilibration of SG (slope/gradient in Figure 2b) is due to smaller concentration gradients inside the particles as the average diameter are much smaller (almost factor 10) for SG (D10/50/90 value = 0.9 µm/2.3 µm/5.7 µm) compared to LG (D10/50/90 value = 7 µm/19 µm/47 µm).

Prior to the measurements, the MLC was cycled with a C/20 formation regime at 25 °C.[18]

## Model

To get a more fundamental understanding of the dominating processes resulting in an inhomogeneous utilization and to discuss possible design implications to improve the homogeneity of utilization, we implemented the MLC design in a model environment using COMSOL Multiphysics 5.2a.

The established model is of a pseudo-two-dimensional (P2D) class as introduced by Newman and co-workers[24,25] and used extensively in literature for different applications.[26–30] This modeling class was chosen for its accuracy in describing transport phenomena in the solid and liquid phase of a single electrode stack.[31] As the P2D model is extensively discussed in literature, we only show the modifications to the basic model and included a short summary with all relevant parameters in the Appendix.

***Particle size distribution.***—For the graphite electrodes we implemented three overlapping domains each with a different distinct particle radius to overcome the restriction made by the P2D approach in homogenizing all particles.[32–35] We used the given D values for the two graphites as the three representative sizes. To not change the overall active volume $V_s$ of the cell, the volumetric share $k_m$ of each particle size needs to be considered.

$$V_s = \sum_m k_m \cdot V_{P,m} \quad [1]$$

The impact of different particle sizes on relaxation has already been shown before by Darling et al.[36] The relatively slow lithium-ion transport inside the particles leads to high gradients especially in large particles. As a realistic distribution, we assumed a volumetric share of 2% for the D10, 67% for the D50 and 31% for the D90 particles as measured by Wilhelm et al.[37]

***Separated electrode model.***—To validate our model to the measured data, we first implemented just one electrode domain with a thickness of 132 µm which corresponds to adding up the three 44 µm electrode disks from the MLC. At the theoretical tab positions we included a measurement probe to compare the behavior to the MLC measurement data. As this model featured the observed inhomogeneous lithium-ion retrieval qualitatively but not in its actual distinctness, we extended the model by implementing the three electrode domains and the in-between separator domains separately. This lead to a better agreement of simulation and measurement data as transport limitations in the additional lengths of the separators were included. Another advantage was that the three electrode simulation enabled to distinguish between the relaxation effects (I) and (II). A comparison between the two modeled geometries and inherent data can be seen in Figure 3.

As the active domains with the charge-transfer reaction were separated, a single current density source boundary condition at $x = L$ was not sufficient. To allow for a collective current flow from all three electrodes and equilibration currents between the layers after stopping the overall current, the domains need to be coupled by extra boundary conditions. This coupling of three electronically separated electrodes in a one-dimensional model, where the boundary conditions mimic an external circuitry, has to our knowledge not been published yet and will be introduced in the following.

Figure 4 depicts all necessary potential and current definitions for the coupled operation. The overall applied current density $i_{app}$ is split

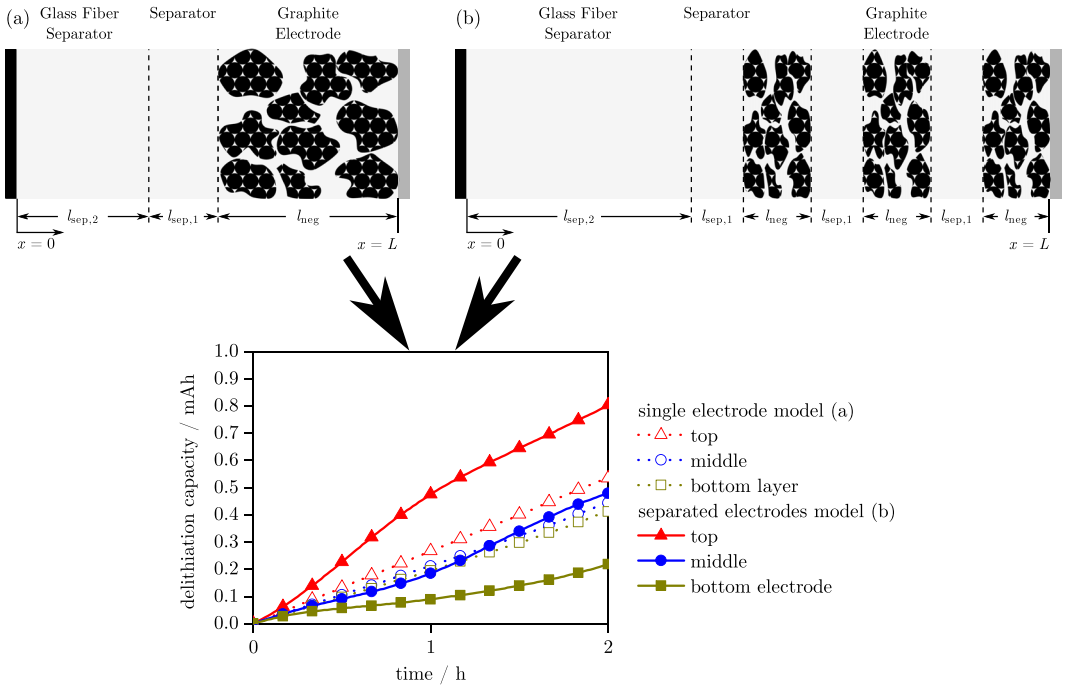


**Figure 3.** Comparison of modeling with (a) single thick electrode and (b) three separated electrodes.

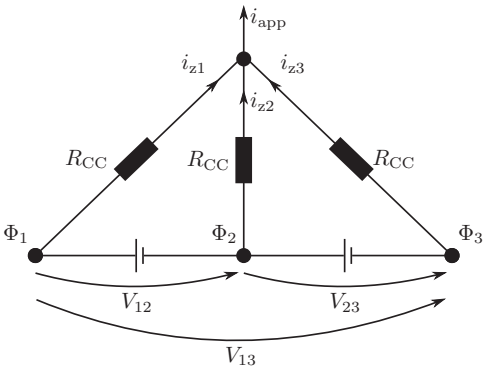


**Figure 4.** Depiction of potential and current definitions used in the coupling of the three separated electrode layers.

in a current for each layer $i_{z,i}$

$$i_{app} = \sum_i i_{z,i} \quad [2]$$

The voltage $V_{ij}$ in-between the separated layers is defined by the difference in their respective average potential at the current collector $\Phi_i$ and $\Phi_j$

$$V_{ij} = \Phi_i - \Phi_j \quad [3]$$

Applying Kirchhoff's laws to the scheme in Figure 4, the current density for each layer is dependent on the current density of the next layer, their voltage difference and the connection through a current collector ($R_{CC}$) which is assumed the same for all layers

$$i_{z,i} = i_{z,j} + \frac{V_{ij}}{R_{CC}} \quad [4]$$

We can sum up the model development part by stating that the three electrode modeling approach is superior in terms of matching the actual measurements to simulation results, although the thick single electrode approach is already sufficient to predict the degree of homogeneous utilization in a real application. The agreement of measurement and model data can be seen in Figure 5.

## Results and Discussion

The purpose of developing a model to account for inhomogeneous utilization and following equilibration is being able to examine the extent of influence of different design parameters.

***Identification of influencing parameters.—***Starting with the parametrized three electrode model of LG, we varied parameters describing lithium-ion transport in the electrolyte phase as apparently the transport through the thickness of the electrode poses a limitation. (To achieve a better comparability, the total active material amount stays the same in all simulations, i.e. when increasing the porosity, the electrode length/thickness is also increased.) As the duration of equilibration is directly linked to the inhomogeneity of electrode utilization, Figures 6 and 7 only show the behavior of the retrieved charge from each layer compared to the initial values.

Changes of porosity and tortuosity are expected to have a similar impact on the diffusion coefficient and the electrolyte conductivity as they are scaling the transport parameters to effective values (see Equation A7). To achieve a 10 times larger effective diffusion coefficient of the electrolyte (Figure 6c) without changing the electrolyte

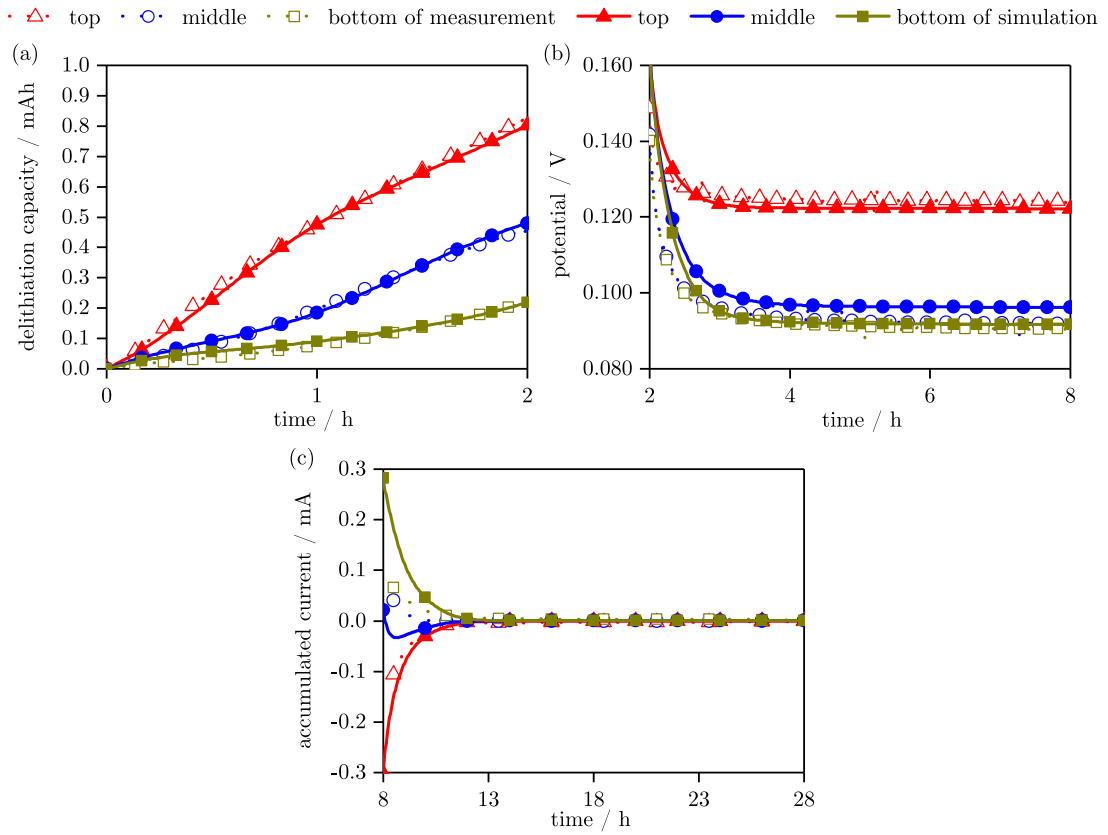


**Figure 5.** Comparison of measurement (hollow markers) and modeling (filled markers) results for MLC with LG particles during delithiation with C/10 rate and subsequent relaxation. (a) depicts the delithiation process of the three electrodes and (b) the intra-particle relaxation phase during which no charge is exchanged between the layers. (c) shows the current flowing during the 29 min inter-particle relaxation phases between the shorted layers (lines are for guidance purposes).

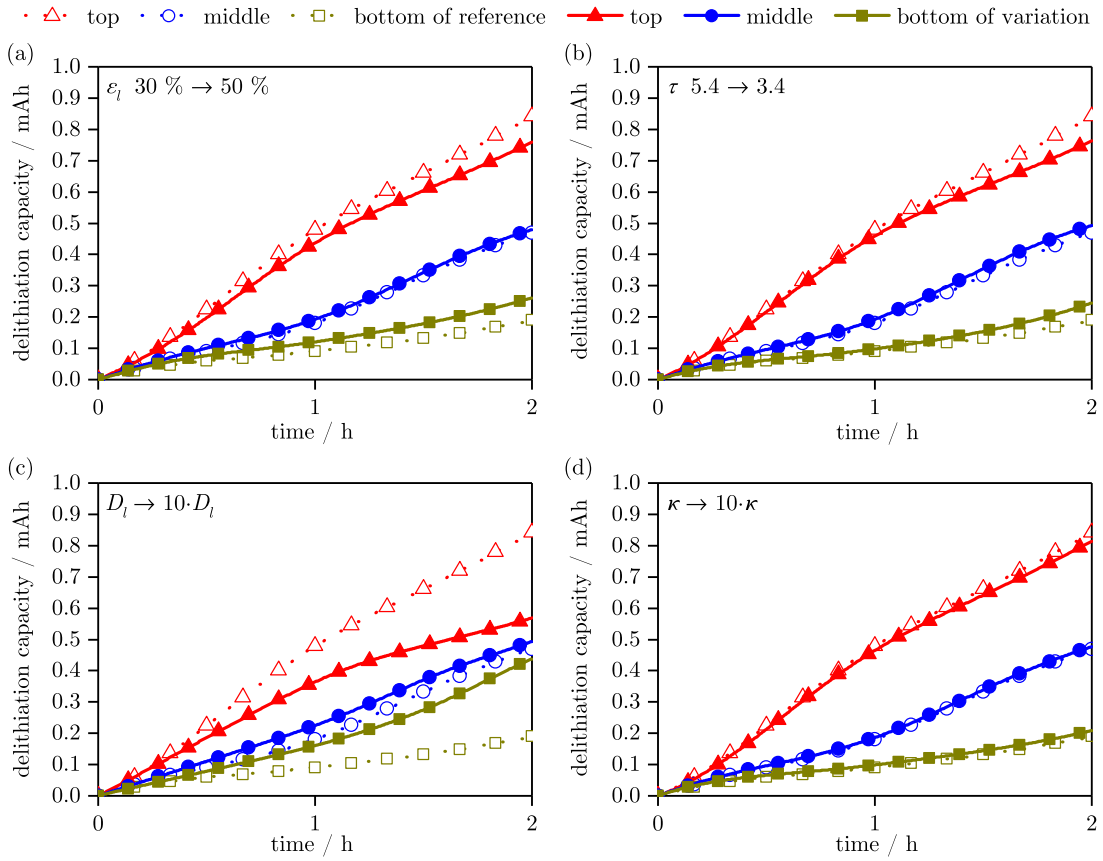


**Figure 6.** Utilization of the three layers by varying parameters regarding the electrolyte phase. The increase in (a) porosity (+20 %) and (b) decrease in tortuosity (−2) only shows minor improvement. Increasing the diffusion coefficient (c) by a factor of 10 shows a drastically more homogeneous utilization whereas the same increase for the conductivity (d) has almost no effect.

itself, the factor $\frac{\varepsilon_l}{\tau}$ would need to be ten times larger. In its extreme scenarios this implies that the porosity would need to increase by a factor of ten (which would result in a porosity larger than 100%) or the tortuosity would need to decrease by a factor of ten (which would result in a tortuosity smaller than 1). As both cases are impossible increasing the diffusion coefficient of the electrolyte itself seems like the only viable option. The fact that the mass and charge transport in the electrolyte is mainly diffusion controlled is consolidated as the increase in electrolyte conductivity shows no significant improvement (Figure 6d).

Similar to the comparison of parameters referring to the liquid phase, Figure 7 shows the influence of solid phase parameters. First, we included the particle radii distribution of the SG in the LG parametrized model as that gives a larger reacting surface at otherwise same conditions. As depicted in Figure 7a, this lead to consecutively following behavior where in the beginning the top electrode delivers even more charge which is later followed by the middle electrode. This behavior can be explained by the proportionally larger surface area of the SG that gets delithiated prior to the development of inhomogeneous surface potentials across the electrode that influence the charge-transfer. Increasing the particle radii would lead to a more homogeneous distribution in a first approximation but relaxation times would also rise significantly and are therefore left out of further discussions. Doubling the reaction rate constant – we assume the reaction rate constant as a parameter of the solid phase as the electrolyte is the same in all prior experiments – to allow for a faster (de-)intercalation of lithium-ions also leads to a slightly more inhomogeneous utilization as charge-transfer is encouraged even though there is a smaller driving potential. Similar to the change in reaction rate constant, increasing the diffusion coefficient in the graphite by a factor of 100 to allow for a faster homogenization inside the particle has only a minor effect as the overall limitations originate from the liquid phase transport.

To summarize the study of influencing parameters, we see that the parameters influencing the effective electrolyte diffusivity have the biggest impact on the homogeneity of current density distribution across an electrode.

***Variation of electrode design for more homogeneous current density distribution.—***Following the parameter analysis, we varied porosity, tortuosity and particle radii in the different layers to find a more homogeneous utilization by electrode design variation. The parameter combinations of the variation studies can be seen in Table II and the results are depicted in Figure 8. Primary modeling results showed a better utilization when using LG near the separator and SG near the current collector, so this is assumed in all following variations. An opposite distribution discharges the SG even faster due to the larger surface.[32] In addition to the previously introduced SG and LG samples, we modeled a made-up medium sized graphite (MG) for the variation studies that has a D10 value of 3.9 µm, a D50 value of 10.7 µm and a D90 value of 26.4 µm. Also, the effective thickness of the electrode layer varies in order to keep a constant area specific capacity per electrode layer with changing porosities. The overall thickness of all three electrodes is then in the range of 150 µm to 200 µm which is in the order of the goal for future high-energy cells.[38]

The first variation between variation study model 1 (VSM1) and 2 (VSM2) is a change in porosity. Whereas VSM1 has a decreasing porosity from top to bottom, VSM2 incorporates an increase. In Figure 8 we see a slightly more homogeneous utilization from (a) to (b). This is based on a larger reservoir of electrolyte within the pores near the current collector which dominates the rate limitation due to

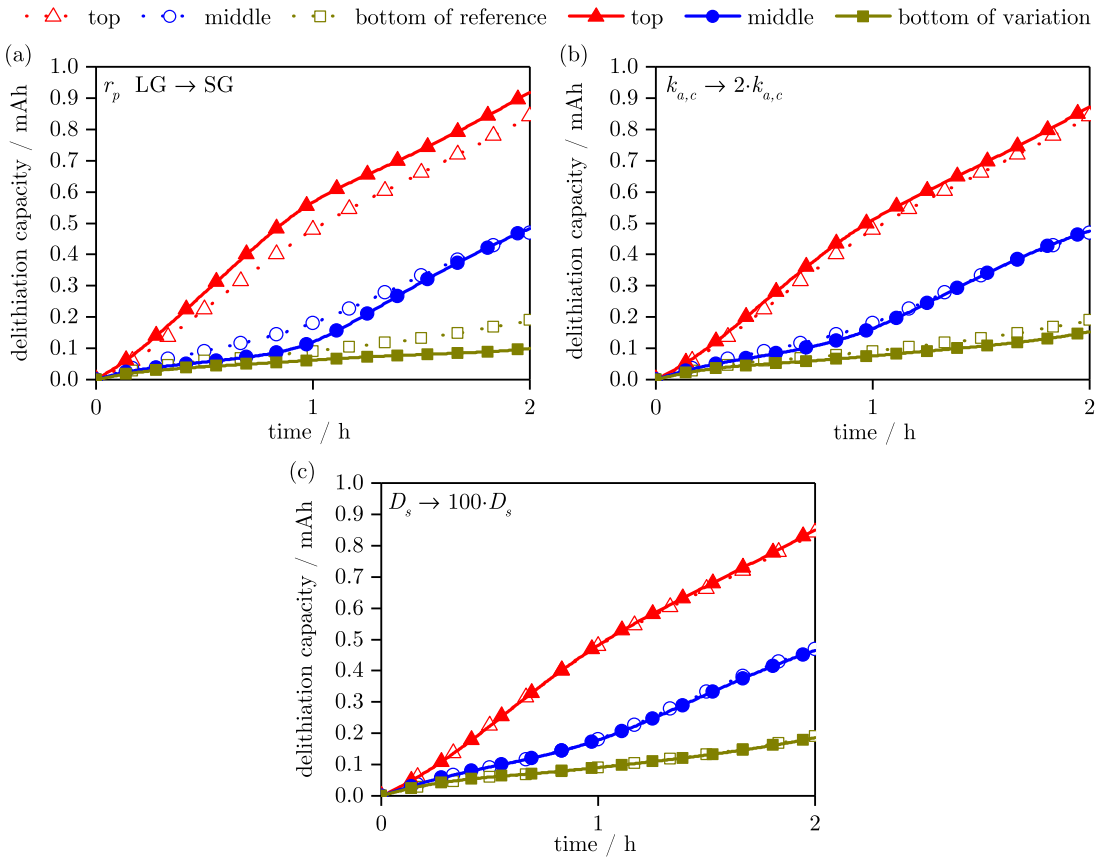


**Figure 7.** Reducing the particle radii by almost a factor of ten leads to an even more inhomogeneous, wave-like utilization (a). Doubling the reaction rate constant (b) or increasing the solid phase diffusion coefficient by a factor of 100 (c) shows a minor influence.

lithium-ion depletion (i.e. $c_l = 0$) as also suggested by e.g. Gallagher et al.[38]

A correlation of higher porosity leading to lower tortuosity was tested in VSM3. Compared to a more theoretical inverse correlation in VSM4, we can see better results for VSM4 in Figure 8c and 8d. The compensation of a lower porosity by a low tortuosity in VSM4 outperforms the very good effective transport parameters of the middle and bottom electrode of VSM3.

Based on the previous findings, we decreased the overall tortuosity which could represent an electrode morphology modified (i.e. structured) after coating and calendaring with the aid of a laser beam to include "pore channels" through the electrode layer similar to the idea proposed by Bae et al.[39] As can be seen for VSM5 in Figure 8e, this bi-tortuos electrode morphology – which also leads to an increase in porosity due to extraction of material – allows for a considerably better electrode utilization. With VSM6, we investigated the actual impact of porosity for a pore channel electrode and simplified the assumption to a uniform 50%. By comparing Figure 8e and 8f, we see that the exact porosity has only a minor impact but that a structured electrode improving the overall tortuosity benefits a homogeneous utilization even in case of an almost 200 µm thick electrode.

**Table II. Parameter combinations for the variation study models (VSM).**

| | Reference | VSM1 | VSM2 | VSM3 | VSM4 | VSM5 | VSM6 |
|---|---|---|---|---|---|---|---|
| **Top electrode** | | | | | | | |
| Porosity $\varepsilon_l$ | 30% | 50% | 30% | 30% | 30% | 40% | 50% |
| Tortuosity $\tau$ | 5.4 | 5.4 | 5.4 | 5.4 | 3.4 | 1.4 | 1.4 |
| Particles | LG | LG | LG | LG | LG | LG | LG |
| Effective thickness | 44.0 µm | 64.0 µm | 44.0 µm | 44.0 µm | 44.0 µm | 52.1 µm | 64.0 µm |
| **Middle electrode** | | | | | | | |
| Porosity $\varepsilon_l$ | 30% | 40% | 40% | 40% | 40% | 50% | 50% |
| Tortuosity $\tau$ | 5.4 | 5.4 | 5.4 | 4.4 | 4.4 | 2.4 | 2.4 |
| Particles | LG | MG | MG | MG | MG | MG | MG |
| Effective thickness | 44.0 µm | 52.1 µm | 52.1 µm | 52.1 µm | 52.1 µm | 64.0 µm | 64.0 µm |
| **Bottom electrode** | | | | | | | |
| Porosity $\varepsilon_l$ | 30% | 30% | 50% | 50% | 50% | 60% | 50% |
| Tortuosity $\tau$ | 5.4 | 5.4 | 5.4 | 3.4 | 5.4 | 3.4 | 3.4 |
| Particles | LG | SG | SG | SG | SG | SG | SG |
| Effective thickness | 44.0 µm | 44.0 µm | 64.0 µm | 64.0 µm | 64.0 µm | 82.8 µm | 64.0 µm |

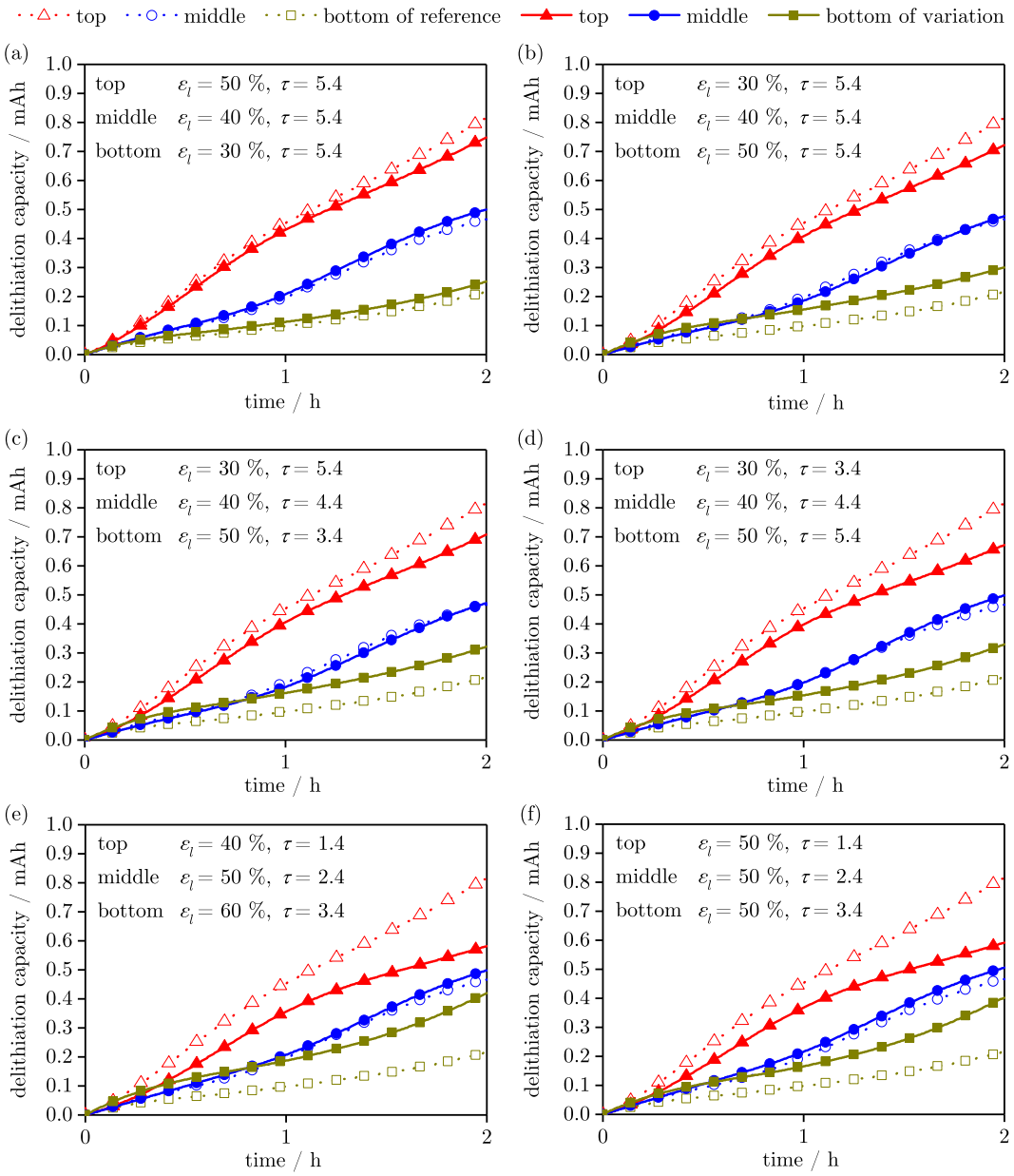


**Figure 8.** Effects of parameter variation studies as shown in Table II. (a)–(f) corresponds to VSM1–VSM6 and dashed lines represent the utilization of the reference for comparison.

To check if our variation shows a better performance, we simulated a rate capability test for electrodes in a normal (lithium-metal electrode//Celgard separator//graphite electrode) half-cell setup with parameters of the reference model and VSM6. As can be seen in Figure 9 the VSM6 electrode performs significantly better compared to the reference model electrode. A diffusion limitation at a C-rate higher than 0.6 C can be observed. Nevertheless this is still superior to the 0.2 C limitation seen for the reference.

In future work, we will try to experimentally verify the findings regarding the impact of electrode structure on rate capability. At the moment, we still face problems of manufacturing the appropriate electrodes.

## Conclusions

In this paper, we parametrized a P2D model with three distinctive particle sizes to account for relaxation process in a laboratory, multi-layer cell design for a graphite half-cell. Two in particle size different graphites were investigated and implemented. For reproducing the actual withdrawn capacity from each layer of the MLC, we introduced a coupling procedure that had not been shown before.

Within our model we saw that smaller particles equilibrate faster due to their higher surface to volume ratio. For a homogeneous utilization, liquid phase parameters such as porosity, tortuosity and the diffusion coefficient of the electrolyte showed a higher impact than e.g. solid phase diffusion.

During the variation studies carried out with the aid of the model, it was observed that smaller graphite particles are beneficial near the current collector and larger particles near the separator toward the counter electrode. Also a porosity increase from separator to current collector showed a better utilization as the hard to reach pores near the current collector present a larger reservoir for lithium-ions which postpones rate limitation toward higher C-rates (compare VSM1 and VSM2). The biggest improvement was achieved by reducing the

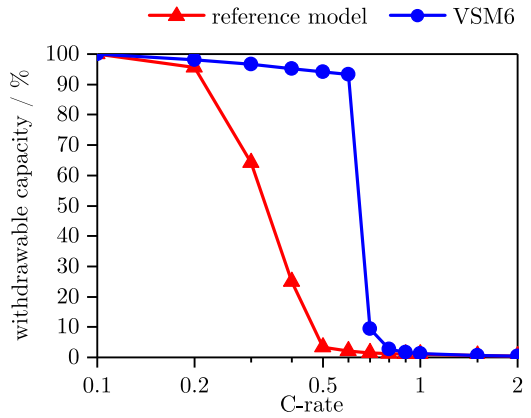


**Figure 9.** Comparison of reference and VSM6 electrode in a rate capability test. The withdrawable capacity is normalized to the capacity at 0.1 C. The sudden decrease in withdrawable capacity can be attributed to diffusion limitations in the electrolyte.

tortuosity overall and from separator to current collector (VSM3 to VSM5). The latter case could be implemented by including pore channels into the graphite electrode by means of laser beam structuring after the coating and calendering process during manufacturing.

In conclusion, the structuring of electrodes is a promising way to achieve a more homogeneous utilization in thick electrodes for high energy cells. The more homogeneous utilization during operation will lead to shorter equalization times and also to a more homogeneous aging behavior as that is largely caused by the current density distribution.

## Acknowledgment

The support for this by the German Federal Ministry of Education and Research in the projects *EffiForm* (03XP0034G) and *ExZellTUM* (03X4633A) is greatly appreciated. The authors thank Prof. Wolfgang Schuhmann from Ruhr-University Bochum for lending them the multi-layer cell and Prof. Hubert A. Gasteiger at TUM for providing laboratory facilities. They also thank SGL Carbon GmbH for supplying the used graphites and Prof. Jürgen Garche for the auxiliary discussions during composition of this paper.

## Appendix

***Basics of P2D model.***—The P2D model is based on porous electrode and concentrated solution theory and solves lithium-ion concentration $c_i$ and potential $\Phi_i$ within the liquid electrolyte (subscript $i = l$) and the solid active material (subscript $i = s$) phase. The model geometry is defined as a one dimensional interval divided into two main domains corresponding to the separator and the graphite electrode. An additional dimension is set for the description of species intercalation within the particle domain. For a detailed model description, the reader is referred to Reference 27. The main equations are mass balance for lithium-ions in the electrolyte $c_l$

$$\varepsilon_l \frac{\partial c_l}{\partial t} = \nabla \left( D_{l,eff} \nabla c_l - \frac{\boldsymbol{i}_l t_+}{F} \right) + a_s j_n \qquad [A1]$$

and charge balance

$$\nabla \left( -\kappa_{eff} \nabla \Phi_l + \frac{2\kappa_{eff} RT}{F} \left( 1 + \frac{\partial \ln f_\pm}{\partial \ln c_l} \right) (1 - t_+) \nabla \ln c_l \right) = F a_s j_n \qquad [A2]$$

throughout the electrode domain. The current within the liquid phase is described by the current density $\boldsymbol{i}_l$ and potential $\Phi_l$, while the pore wall flux at the electrode-electrolyte interface is named $j_n$. $R$ describes the universal gas constant, $F$ the Faraday's constant and $T$ the local absolute temperature which is kept constant in this case. Within the separator domain the equations simplify to

$$\varepsilon_l \frac{\partial c_l}{\partial t} = \nabla \left( D_{l,eff} \nabla c_l - \frac{\boldsymbol{i}_l t_+}{F} \right) \qquad [A3]$$

and

$$\nabla \left( -\kappa_{eff} \nabla \Phi_l + \frac{2\kappa_{eff} RT}{F} \left( 1 + \frac{\partial \ln f_\pm}{\partial \ln c_l} \right) (1 - t_+) \nabla \ln c_l \right) = 0 \qquad [A4]$$

To couple solid and liquid phase, Butler-Volmer kinetics are assumed for the pore wall flux

$$j_n = k_c^{\alpha_a} k_a^{\alpha_c} \left( c_{s,max} - c_s|_{r=r_p} \right)^{\alpha_a} \left( c_s|_{r=r_p} \right)^{\alpha_c} \left( \frac{c_l}{1\,\mathrm{mol\,m^{-3}}} \right)^{\alpha_a} \left( e^{\frac{\alpha_a F}{RT}\eta} - e^{-\frac{\alpha_c F}{RT}\eta} \right) \qquad [A5]$$

including the lithium-ion concentration at the particle's surface $c_s$ and the overpotential

$$\eta = \Phi_s - \Phi_l - E_{\mathrm{Eq}} \qquad [A6]$$

where $\Phi_s$ corresponds to the solid phase potential.

Effective transport parameters are used to account for tortuosity in the homogenized P2D model by scaling material parameters with a function of porosity $\varepsilon_l$ and tortuosity $\tau$[40]

$$\Psi_{l,eff} = \frac{\varepsilon_l}{\tau} \Psi_l \qquad [A7]$$

To describe the electrolyte's characteristics properly, a concentration dependence is implemented for conductivity, diffusivity and mean molar activity coefficient of the electrolyte. These are taken from fittings to measurements[41] while presuming a constant transport number. The applied diffusion coefficients are estimated from various literature sources.[26,27,30,42] The equilibrium potential is taken from literature[42] as well as the maximum concentration of lithium within the active material particles.[42,43] Additional parameters such as reaction rate constants[30,42] are assumed based on references from literature. The chosen parameters measured or taken from literature are summarized in Table AI and AII.

**Table AI. Physicochemical parameters for the two graphites. Superscript *m* indicates measured values and superscript *e* values estimated from literature.**

| Parameter | SG | LG |
|---|---|---|
| **Geometry** | | |
| Solid phase fraction $\varepsilon_s$ | 0.15 $^m$ | 0.62 $^m$ |
| Liquid phase fraction $\varepsilon_l$ | 0.79 $^m$ | 0.3 $^m$ |
| Tortuosity $\tau$ | 3.7 $^m$ | 5.4 $^m$ |
| **Thermodynamics** | | |
| Equilibrium voltage $E_{\mathrm{Eq,neg}}$ | *analytic term*[42]; see Equation A8 | |
| Maximum lithium concentration $c_{s,max}$ | 30555 mol/m$^3$ $^e$ | 30555 mol/m$^3$ $^e$ |
| Initial state of charge $\frac{c_{s,0}}{c_{s,max}}$ | 0.75 $^e$ | 0.7 $^e$ |
| **Kinetics** | | |
| Reaction rate constant $k_{a,c}$ | $4 \times 10^{-11}$ m/s $^e$ | $2 \times 10^{-11}$ m/s $^e$ |
| Anodic charge-transfer coefficient $\alpha_a$ | 0.5 $^e$ | 0.5 $^e$ |
| Cathodic charge-transfer coefficient $\alpha_c$ | 0.5 $^e$ | 0.5 $^e$ |
| **Transport** | | |
| Solid diffusivity $D_s$ | $3.9 \times 10^{-14}$m$^2$/s $^e$ | $3.9 \times 10^{-14}$m$^2$/s $^e$ |
| Solid conductivity $\sigma$ | 100 S/m $^e$ | 100 S/m $^e$ |
| SEI resistance $R_{\mathrm{SEI}}$ | 0.001 $\Omega^2$m $^e$ | 0.001 $\Omega^2$m $^e$ |

**Table AII. Additional model parameters applicable for both graphites.**

| Parameter | Value |
|---|---|
| **Electrolyte** | |
| Electrolyte diffusivity $D_l$ | *analytic term*[41]; see equation A9 |
| Electrolyte conductivity $\kappa$ | *analytic term*[41]; see equation A10 |
| Activity dependency $\frac{\partial \ln f_{\pm}}{\partial \ln c_l}$ | *analytic term*[41]; see equation A11 |
| Transport number $t_+$ | 0.363[41] |
| **Separator** | |
| Celgard separator thickness $l_{sep,1}$ | 25 µm |
| Celgard separator porosity $\varepsilon_{Celgard}$ | 0.39[23] |
| Celgard separator tortuosity $\tau_{Celgard}$ | 4.1[23] |
| Glass fiber separator thickness $l_{sep,2}$ | 260 µm |
| Glass fiber separator porosity $\varepsilon_{GF}$ | 0.6 [m] |
| Glass fiber separator tortuosity $\tau_{GF}$ | 2.7 [m] |
| **Additional** | |
| Temperature $T$ | 25 °C |

Equilibrium voltage curve for graphite as a function of lithiation degree $x$. The original definition by Safari et al.[42] is increased by 5 mV to agree with our graphite measurements.

$$E_{Eq,neg} = 0.6379 + (0.5416\exp(-305.5309x)) + 0.044\tanh\left(\frac{-x+0.1958}{0.1088}\right) - 0.1978\tanh\left(\frac{x-1.0571}{0.0854}\right) - 0.6875\tanh\left(\frac{x+0.0117}{0.0529}\right) - 0.0175\tanh\left(\frac{x-0.5692}{0.0875}\right) \quad [A8]$$

Analytical dependencies for electrolyte diffusivity $D_l$, conductivity $\kappa$ and activity $\frac{\partial \ln f_{\pm}}{\partial \ln c_l}$ as functions of temperature $T$, lithium-ion concentration in the liquid phase $c_l$ and transport number $t_+$ as measured by Valøen et al.[41] The electrolyte diffusivity was scaled to 0.3 as the used electrolyte had a lower diffusivity compared to the one used by Valøen which is still in the order of known diffusivity values.[44]

$$D_l = 0.3 \times \left(10^{-4.43-\frac{54}{T-(229+5c_l)}-0.22c_l} \times 10^{-4}\right) \quad [A9]$$

$$\kappa = 0.1c_l\Big(-10.5 + 0.074T - 6.96\times10^{-2}T^2 + 0.668c_l - 0.0178c_lT + 2.8\times10^{-5}c_lT^2 + 0.494c_l^2 - 8.86\times10^{-4}c_l^2T\Big)^2 \quad [A10]$$

$$\frac{\partial \ln f_{\pm}}{\partial \ln c_l} = \frac{0.601 - 0.24c_l^{0.5} + 0.982c_l^{1.5}(1-0.0052(T-294))}{1-t_+} - 1 \quad [A11]$$

## References


1. B. Scrosati and J. Garche, *Journal of Power Sources*, **195**, 2419 (2010).
2. A. E. Trippe, R. Arunachala, T. Massier, A. Jossen, and T. Hamacher, *IEEE PES Innovative Smart Grid Technologies Conference Europe*, 1 (2014).
3. Tesla, Supercharger. 2017; https://www.tesla.com/supercharger.
4. G. Zhang, C. E. Shaffer, C.-Y. Wang, and C. D. Rahn, *Journal of the Electrochemical Society*, **160**, A610 (2013).
5. P. J. Osswald, S. V. Erhard, J. Wilhelm, H. E. Hoster, and A. Jossen, *Journal of the Electrochemical Society*, **162**, A2099 (2015).
6. P. J. Osswald, S. V. Erhard, A. Rheinfeld, B. Rieger, H. E. Hoster, and A. Jossen, *Journal of Power Sources*, **329**, 546 (2016).
7. S. J. Harris and P. Lu, *The Journal of Physical Chemistry C*, **117**, 6481 (2013).
8. S. J. Harris, A. Timmons, D. R. Baker, and C. W. Monroe, *Chemical Physics Letters*, **485**, 265 (2010).
9. K. Kitada, H. Murayama, K. Fukuda, H. Arai, Y. Uchimoto, Z. Ogumi, and E. Matsubara, *Journal of Power Sources*, **301**, 11 (2016).
10. H. Abe, M. Kubota, M. Nemoto, Y. Masuda, Y. Tanaka, H. Munakata, and K. Kanamura, *Journal of Power Sources*, **334**, 78 (2016).
11. H. Tanida, H. Yamashige, Y. Orikasa, Y. Gogyo, H. Arai, Y. Uchimoto, and Z. Ogumi, *The Journal of Physical Chemistry C*, **120**, 4739 (2016).
12. S. V. Erhard, P. J. Osswald, J. Wilhelm, A. Rheinfeld, S. Kosch, and A. Jossen, *Journal of the Electrochemical Society*, **162**, A2707 (2015).
13. S. V. Erhard et al., *Journal of the Electrochemical Society*, **164**, A6324 (2017).
14. V. Zinth, C. von Lüders, M. Hofmann, J. Hattendorff, I. Buchberger, S. V. Erhard, J. Rebelo-Kornmeier, A. Jossen, and R. Gilles, *Journal of Power Sources*, **271**, 152 (2014).
15. C. von Lüders, V. Zinth, S. V. Erhard, P. J. Osswald, M. Hofmann, R. Gilles, and A. Jossen, *Journal of Power Sources*, **342**, 17 (2017).
16. B. Rieger, S. F. Schuster, S. V. Erhard, P. J. Osswald, A. Rheinfeld, C. Willmann, and A. Jossen, *Journal of Energy Storage*, **8**, 1 (2016).
17. F. M. Kindermann, A. Noel, S. V. Erhard, and A. Jossen, *Electrochimica Acta*, **185**, 107 (2015).
18. F. M. Kindermann, P. J. Osswald, S. Klink, G. Ehlert, J. Schuster, A. Noel, S. V. Erhard, W. Schuhmann, and A. Jossen, *Journal of Power Sources*, **342**, 638 (2017).
19. F. La Mantia, Characterization of Electrodes for Lithium-Ion Batteries through Electrochemical Impedance Spectroscopy and Mass Spectrometry: Nr. 17848. Ph.D. thesis, ETH Zürich, Zürich, 2008.
20. S.-H. Ng, F. La Mantia, and P. Novák, *Angewandte Chemie (International edition)*, **48**, 528 (2009).
21. S. Klink, W. Schuhmann, and F. La Mantia, *ChemSusChem*, **7**, 2159 (2014).
22. S. Klink, P. Weide, M. Muhler, W. Schuhmann, and F. La Mantia, *ECS Transactions*, **62**, 265 (2014).
23. J. Landesfeind, A. Ehrl, M. Graf, W. A. Wall, and H. A. Gasteiger, *Journal of the Electrochemical Society*, **163**, A1254 (2016).
24. J. S. Newman and C. W. Tobias, *Journal of the Electrochemical Society*, **109**, 1183 (1962).
25. J. S. Newman and K. E. Thomas-Alyea, *Electrochemical systems*, 3rd ed.; Wiley-Interscience: Hoboken, NJ, 2004.
26. C. M. Doyle, T. F. Fuller, and J. S. Newman, *Journal of the Electrochemical Society*, **140**, 1526 (1993).
27. T. F. Fuller, C. M. Doyle, and J. S. Newman, *Journal of the Electrochemical Society*, **141**, 982 (1994).
28. T. R. Ashwin, Y. M. Chung, and J. Wang, *Journal of Power Sources*, **328**, 586 (2016).
29. M. Ecker, T. K. D. Tran, P. Dechent, S. Käbitz, A. Warnecke, and D. U. Sauer, *Journal of the Electrochemical Society*, **162**, A1836 (2015).
30. S. G. Stewart, V. Srinivasan, and J. S. Newman, *Journal of the Electrochemical Society*, **155**, A664 (2008).
31. A. Jokar, B. Rajabloo, M. Désilets, and M. Lacroix, *Journal of the Electrochemical Society*, **163**, A2876 (2016).
32. G. S. Nagarajan, J. W. van Zee, and R. M. Spotnitz, *Journal of the Electrochemical Society*, **145**, 771 (1998).
33. Z. Mao, M. Farkhondeh, M. Pritzker, M. Fowler, and Z. Chen, *Journal of the Electrochemical Society*, **163**, A458 (2015).
34. P. Albertus, J. Christensen, and J. S. Newman, *Journal of the Electrochemical Society*, **156**, A606 (2009).
35. M. Ender, *Journal of Power Sources*, **282**, 572 (2015).
36. R. B. Darling and J. S. Newman, *Journal of the Electrochemical Society*, **144**, 4201 (1997).
37. J. Wilhelm, S. V. Erhard, I. Buchberger, and A. Jossen, Simulation of Lithium-Ion Battery Equalization Effects. ModVal 13. 2016.
38. K. G. Gallagher, S. E. Trask, C. Bauer, T. Woehrle, S. F. Lux, M. Tschech, P. Lamp, B. J. Polzin, S. Ha, B. Long, Q. Wu, W. Lu, D. W. Dees, and A. N. Jansen, *Journal of the Electrochemical Society*, **163**, A138 (2016).
39. C.-J. Bae, C. K. Erdonmez, J. W. Halloran, and Y.-M. Chiang, *Advanced materials*, **25**, 1254 (2013).
40. M. J. Martínez-Rodríguez, S. Shimpalee, and J. W. Van Zee, *Journal of the Electrochemical Society*, **156**, B80. (2009).
41. L. O. Valøen and J. N. Reimers, *Journal of the Electrochemical Society*, **152**, A882 (2005).
42. M. Safari and C. Delacourt, *Journal of the Electrochemical Society*, **158**, A562 (2011).
43. P. Ramadass, B. S. Haran, P. M. Gomadam, R. E. White, and B. N. Popov, *Journal of the Electrochemical Society*, **151**, A196 (2004).
44. M. Guo and R. E. White, *Journal of Power Sources*, **221**, 334 (2013).